Neurosci. Bull. February, 2016, 32(1):1–15
DOI 10.1007/s12264-016-0012-2

www.neurosci.cn
www.springer.com/12264

ORIGINAL ARTICLE

Actin Aggregations Mark the Sites of Neurite Initiation

Shu-Xin Zhang[1,2] · Li-Hui Duan[1,2] · Hong Qian[3] · Xiang Yu[1]

Received: 29 September 2015 / Accepted: 25 November 2015 / Published online: 18 January 2016

Abstract A salient feature of neurons is their intrinsic ability to grow and extend neurites, even in the absence of external cues. Compared to the later stages of neuronal development, such as neuronal polarization and dendrite morphogenesis, the early steps of neuritogenesis remain relatively unexplored. Here we showed that redistribution of cortical actin into large aggregates preceded neuritogenesis and determined the site of neurite initiation. Enhancing actin polymerization by jasplakinolide treatment effectively blocked actin redistribution and neurite initiation, while treatment with the actin depolymerizing agents latrunculin A or cytochalasin D accelerated neurite formation. Together, these results demonstrate a critical role of actin dynamics and reorganization in neurite initiation. Further experiments showed that microtubule dynamics and protein synthesis are not required for neurite initiation, but are required for later neurite stabilization. The redistribution of actin during early neuronal development was also observed in the cerebral cortex and hippocampus *in vivo*.

Keywords Neurite initiation · Neuritogenesis · Actin aggregations · Actin · Microtubules

Shu-Xin Zhang and Li-Hui Duan have contributed equally to this work.

✉ Xiang Yu
yuxiang@ion.ac.cn

[1] Institute of Neuroscience, State Key Laboratory of Neuroscience, CAS Center for Excellence in Brain Science and Intelligence Technology, Shanghai Institutes for Biological Sciences, Chinese Academy of Sciences, Shanghai 200031, China

[2] University of the Chinese Academy of Sciences, Beijing 100049, China

[3] Department of Applied Mathematics, University of Washington, Seattle, Washington 98195, USA

Introduction

A key characteristic of neurons that distinguishes them from other cell types is their ability to grow and extend neurites, small protrusions or processes initiating from the cell body and extending up to one meter. The ability to extend long and extensive neurites not only morphologically distinguish neurons from other cell types, but also endows them with unique physiological functions, including the ability to reliably transfer electrical signals over long distances, the capacity to integrate information from multiple sources, and the capability to build expansive and intricately connected networks. None of these functions, all hallmarks of neurons, could be achieved without neurite formation.

Classical live imaging studies using cultured neurons have divided neuronal morphogenesis into the following 5 stages: (1) initially, sphere-like neurons develop circumferential lamellipodial and/or filopodial structures shortly after birth or after being plated in culture; (2) the lamellipodia protrude forward, and stable filopodia grow into short, immature neurites; (3) one of the several short neurites develops a large growth cone and rapidly elongates into the axon, thereby establishing neuronal polarity; (4) axons and dendrites differentiate, grow, and branch rapidly; and (5) neurons make synaptic connections, develop dendritic spines, and establish neuronal circuits [1, 2]. These processes, initially described for cultured embryonic hippocampal neurons, have since been generalized to multiple neuronal types both *in vitro* and *in vivo*, with the important difference that in the *in vivo* context,

neuronal morphogenesis occurs concurrently with migration [3–5]. Over the past several decades, studies have mostly focused on the molecular mechanisms underlying the later stages of neuronal morphogenesis, including those mediating polarization [6–9], dendrite morphogenesis [10–16], synaptogenesis [17–20], and spinogenesis [21–24].

Compared to our understanding of the mechanisms mediating the later stages of neuronal morphogenesis, much less is known regarding its earlier stages, especially how a neuron reshapes itself from a spherical, apparently symmetrical cell, to one extending multiple neurites [25–27]. The process of neuritogenesis, or neurite formation, is temporally and mechanistically interwoven with that of neuronal polarization, and also with neuronal migration *in vivo*, as these processes often occur concurrently or sequentially, depending on the cell type. For instance, retinal ganglion cells inherit their apico-basal polarity from the retinal neuroepithelium and develop dendrites and axons respectively from their apical and basal processes, thereby completing the process of polarization at the two-neurite stage or arguably even before neurite initiation [5, 28]. Neocortical pyramidal neurons, on the other hand, undergo a multipolar stage shortly after birth, before becoming bipolar again during radial migration, with a leading dendrite and a trailing axon [29, 30]; additional dendrites grow after the neuron has migrated to its designated location in the neuronal circuit.

Mechanistically, neuritogenesis has been proposed to occur *via* two possible and non-mutually exclusive mechanisms [26, 27, 31–33]. In the convergent elongation model, circumferential lamellipodia collapse at discrete positions and concurrently extended at others, resulting in nascent growth cones that subsequently develop into neurites. This model emphasizes the molecular attachment-and-detachment of lamellipodia to their substratum. In the alternative *de novo* filament formation model, a single filopodium gives rise to a neurite in the absence of discernable lamellipodial protrusions. This model focuses more on internal molecular structural building. Both mechanisms require a break of symmetry in the initially spherical cell body and the formation of an actin-rich filopodium from the cell body, followed by microtubule entry and broadening of the filopodium into a neurite. Earlier work on the mechanism of neurite formation also suggested an important role of microtubule-associated proteins (MAPs) by demonstrating that over-expression of MAP2c in hepatoma cells, in conjunction with pharmacological actin depolymerization, induced the formation of neurite-like structures [34]. Consistently, antisense depletion of MAP2 inhibited neurite initiation [35]. However, other work showed that contact-induced neurite formation in sympathetic neurons still took place in the presence of microtubule stabilizing/destabilizing pharmacological agents [36], and that neurite initiation still occurred in mice double knockout for MAP2 and MAP1B [37], suggesting alterative/redundant mechanisms for neurite initiation. Based on the ability of MAPs to interact with actin, coordination between the two cytoskeletal structures has been proposed to mediate neurite initiation [38, 39]. Similarly, other proteins with the ability to interact with both actin and microtubules have been proposed to play important roles during neurite initiation [26, 27, 32].

As for the role of the actin cytoskeleton, although earlier work suggested that the actin depolymerizing drug cytochalasin D did not inhibit neurite formation in chick dorsal root ganglia neurons [40], more recent studies have demonstrated a critical role of the Ena/Mena/VASP family of proteins (abbreviated as Ena/VASP) in neurite formation [41, 42]. Ena/VASP proteins regulate actin dynamics by antagonizing actin filament capping and promoting filament bundling [43, 44]. In mice lacking all three Ena/VASP proteins, cortical neurons lacked filopodia and failed to initiate neurites, a process that can be rescued either by over-expression of the actin nucleating protein mDia2 or by plating neurons on the filopodia-promoting laminin substrate [41]. In another recent study, the actin depolarizing factor (ADF)/Cofilin family, which depolymerizes and severs actin filaments [45, 46], was shown to promote neurite formation by driving actin retrograde flow and thereby allowing microtubule protrusion [47]. Similarly, polarized actin dynamics has been shown to mark the site of first polarization in round cells [48].

Together, recent work points to a predominant role of the actin cytoskeleton, rather than microtubules, in neurite initiation, with different studies emphasizing either a requirement for actin polymerization or severing. Since the actin studies were carried out using mice with different genetic deletions, and the earlier microtubule studies were performed using peripheral neurons or cell lines, to better understand the relative contribution of the different cytoskeletal components, it is critical to perform all experiments side-by-side in the same culture system. Here, taking advantage of the extensive and well-characterized pharmacological agents available for manipulating cytoskeletal dynamics, we systematically examined the role of the actin cytoskeleton and microtubules in neurite initiation. Using these results, together with those of live-imaging studies and *in vivo* examinations, we provide a more detailed description of the process of neurite initiation.

Materials and Methods

Hippocampal Neuronal Cultures

All animal procedures were approved by the Animal Care and Use Committee of the Institute of Neuroscience, Chinese Academy of Sciences (Shanghai, China). High-density

mixed neuronal-glial cultures were prepared from Sprague-Dawley rat pups on postnatal day 0 (P0) as previously described [49, 50]. Briefly, hippocampi, with the dentate gyri removed, were dissected, and dissociated neurons were plated on glass coverslips (63-3009, Assistent, Sondheim/Rhön, Germany) coated with PDL (P6407, Sigma-Aldrich, St. Louis, MO) at 15,000 neurons per cm^2 in Neurobasal medium (Thermo Fisher Scientific, Waltham, MA) containing B-27 (17504-044, Thermo Fisher Scientific), 2 mmol/L Glutamax-I (35050-061, Thermo Fisher Scientific), and 2.5% FBS (GE Healthcare Life Sciences, Pittsburgh, PA). For live-imaging experiments, neurons were plated on Matrigel (354234, BD Biosciences, Sparks, MD)-coated glass-bottom dishes at 35,000 neurons per cm^2.

For dentate granule cell cultures, only the dentate gyrus was cultured, and Prox 1 immunostaining was used to confirm the identity of the granule cells.

Confocal Microscopy and Structured Illumination Microscopy (SIM)

Confocal images were acquired on one of the following confocal microscopes and objectives: LSM5 (Carl Zeiss, Oberkochen, Germany) with a 63× oil immersion Plan-Apochromat objective (N.A. = 1.4), Nikon A1 plus with a Plan Fluor 40× oil DIC H N2 objective (N.A. = 1.3), or Nikon A1 with a Plan Apo VC 60× oil DIC N2 objective (N.A. = 1.4). Images of large brain sections were acquired with a Zeiss 10× air Fluor objective or Nikon A1 plus with a Plan Apo λ 20× objective (N.A = 0.75).

SIM was performed on an N-SIM microscope (Nikon, Tokyo, Japan), with the CFI Apochromat TIRF 100× oil objective (N.A. = 1.49) and an Andor iXon3 897 EMCCD camera.

Live Cell Imaging

Live imaging experiments were carried out on a Nikon A1R confocal microscope with a Plan Apo VC 60× oil DIC objective (N.A. = 1.4). Imaging sessions started one hour after plating neurons on 35-mm glass-bottom dishes (043520B; Hangzhou Shengyou Biotechnology, Hangzhou, China). The environment was maintained at 37 °C and in 5% CO_2 with a Stage Top incubator (Tokai Hit, Fujinomiya-shi, Japan). Images were acquired hourly with the aid of a motorized stage to mark the position of individual cells.

In Utero Electroporation

Timed-pregnant Sprague-Dawley rats were anesthetized with 3.5 mL/kg of 12% chloral hydrate, and the uterus was carefully exteriorized from the abdominal cavity. Warm saline was used throughout the experiment to prevent dehydration. The lateral ventricles of E15.5 embryos were injected with 2 μL Qiagen Maxiprep DNA and Fast Green dye using a pulled micropipette. The following plasmids were used: pCMV-LifeAct-TagRFP [51] (3 μg/μL; 60102, ibidi GmbH, Martinsried, Germany), GFP-actinin [52] (3 μg/μL), tdTomato [53] (0.5 μg/μL; 22478, Addgene, Cambridge, MA; originally named FUtdTW), and pCS2 min-GFP [49] (1 μg/μL). Forceps-type electrode paddles controlled by an ECM 830 electroporator (BTX Instrument Division, Harvard Apparatus Inc, Holliston, MA) were used to deliver 5 pulses at 60 mV with 50 ms duration at 100 ms intervals. For live imaging experiments, the electroporated cortical hemisphere from P0 pups was cultured. To visualize GFP-actinin localization in brain slices, immunohistochemistry was carried out as previously described [54]. GFP antibody was used to enhance the GFP-actinin signal.

Antibodies

The following antibodies were used: class III β-tubulin (Tuj 1, 1:5000, mouse; G7121, Promega, Madison, WI), GFP (1:1000, Rabbit; A11122, Thermo Fisher Scientific, Waltham, MA, USA), Prox1 (1:1000, rabbit; PRB-238C, Covance, Princeton, NJ). Alexa Fluor 488, 568, or 633 secondary antibodies (Thermo Fisher Scientific) and Alexa Fluor 488, 568 Phalloidin (Thermo Fisher Scientific) were used at 1:1000. Neurons were fixed in 4% PFA for 20 min, permeabilized, and processed for immunocytochemistry according to the standard protocol.

Pharmacological Agents

Jasplakinolide (J7473, Thermo Fisher Scientific), latrunculin A (L5163, Sigma-Aldrich), cytochalasin D (C8273, Sigma-Aldrich), nocodazole (M1404, Sigma-Aldrich), paclitaxel (P3456, Thermo Fisher Scientific) and cycloheximide (C4859, Sigma-Aldrich), were dissolved in DMSO. The control of each experiment was the vehicle used to dissolve the drug. If multiple concentrations were used, the vehicle of the highest concentration drug condition was the control. All pharmacological treatments were compared to vehicle control from the same culture preparation.

Image Analysis

For all morphological analyses, images were coded using a computer-generated random number sequences at the time of data acquisition, and all analyses were performed blinded to the experimental condition. All images were analyzed as acquired with no post-acquisition modifications. Only protrusions immune-positive for Tuj 1 and at least 2 μm in length were considered to be neurites. For fluorescent image and western blot examples, brightness/contrast adjustment

within linear ranges and across the entire image were made using ImageJ (NIH, Bethesda, MD) when necessary.

To analyze the GFP-actinin levels in brain slices, the segmented line selection tool of ImageJ was used to draw a line along the circumference of the cell. The selected line was then straightened and divided into 36 equal sections (each section = 10 degrees). GFP-actinin intensity in each of the 36 sections was measured and normalized to that of tdTomato. Quantified data were presented as a 3D heat map, generated using the MatLab (MatLab R2010a, MathWorks, Natick, MA) surf function, each line representing one neuron. Three-dimensional reconstructions were made using Imaris (v8.1.2, Bitplane, Zurich, Switzerland).

G-actin/F-actin Ratio Assay and Western Blotting

The ratio of G-actin to F-actin was measured using the G-actin/F-actin *In Vivo* Assay Biochem Kit (BK037, Cytoskeleton Inc. Denver, CO), according to the manufacturer's instructions. Briefly, neurons were lysed in F-actin stabilizing buffer and centrifuged for 5 min at 350 g to remove cell debris. F-actin was then pelleted by centrifugation at 100,000 g and 37 °C for 1 h, a process during which G-actin remained in the supernatant. F-actin was then re-suspended in F-actin destabilizing buffer on ice, by frequent pipetting. The G-actin and F-actin fractions were then mixed with 5× SDS sample buffer and boiled, run on SDS-PAGE, and immunoblotted for actin (1:10,000, mouse; MAB1501, Millipore, Billerica, MA). Images were quantified using ImageJ as previously described [55].

Statistical Analysis

For morphological data, statistical analyses were carried out using unpaired two-tailed Student's *t* test (for sample pairs) or one-way ANOVA (for groups of three or more conditions) followed by Dunnett's multiple comparison test. Statistical analyses of neuronal stage percentages and Western blots were carried out using two-way ANOVA followed by Bonferroni post-tests. For live-imaging experiments, paired *t* tests were used. Results are shown as mean ± SEM, and *n* refers to the number of cells unless otherwise indicated. All conditions statistically different from control are indicated. $*P < 0.05$; $**P < 0.01$; $***P < 0.001$.

Results

Neurite Initiation Occurs at the Site of Actin Aggregation

To examine the cytoskeletal mechanisms underlying neurite initiation, we first characterized the time course with which hippocampal neurons in our culture system developed. We fixed neurons at various times after plating and used the F-actin binding compound phalloidin to label actin filaments, and an antibody against neuron-specific class III β-tubulin, Tuj 1, to label microtubules and to distinguish neurons from glial cells. We found that freshly-plated neurons were mostly spherical in shape and displayed a thick layer of F-actin directly underneath their surface membrane (Fig. 1A, 0.5 h). Tuj 1 immunostaining was also evenly distributed underneath the cell membrane, and at a slightly lower level, throughout the cytoplasm (Fig. 1A, 0.5 h). Within the next few hours of development, large actin aggregations began to appear at one or both ends of the cell (Fig. 1A, 6 h), a characteristic that was clearly visualized using SIM (Fig. 1B, C). At later time points, such as 18 h after plating, neurons displayed one or more Tuj 1-containing neurites tipped by F-actin-rich growth cones (Fig. 1A, 18 h). At all time points examined, Tuj 1 redistribution lagged that of F-actin. Thus, our results, consistent with those of recent publications [41, 47, 48], suggest a more critical role of the actin cytoskeleton than of microtubules, in neurite initiation.

To further investigate dynamic changes in F-actin during neurite initiation, we electroporated rat cortical neurons *in utero* with Lifeact-RFP, a red fluorescent protein (RFP)-tagged peptide with high affinity for F-actin [51]. Cultures were subsequently prepared from the P0 cortices of electroporated pups and live-imaged shortly after plating. On initial attachment to the substrate, neurons were spherical in shape, with a thick halo of Lifeact-RFP underneath the cell membrane (Fig. 1D, 0 h). In the ensuing several hours, however, Lifeact-RFP began to aggregate at one location beneath the cell surface (Fig. 1D, 3 h and 6 h), a process that usually preceded neurite initiation (Fig. 1D, 7 h). Quantitation of live imaging experiments using three independent culture preparations showed that in 78.5% of cultured neurons, Lifeact-RFP aggregation(s) were observed prior to neurite initiation (Fig. 1E). In the other 21.5% of cases, neurites were formed without detectable Lifeact-RFP aggregation in the previous imaging frame (Fig. 1E), either because actin did not aggregate or because it occurred during the one-hour window between imaging sessions.

Based on the above static and dynamic images from our own study, and working within the framework of the 5 stages of neuronal morphogenesis [1], we subdivided the previously described stage 1 into stages 1a and 1b, with cells in the former stage having a relatively evenly distributed and thick actin cortex, and cells in the latter stage having one or two large actin aggregations (Fig. 1F). Stage 2 is as previously described, with one or two short Tuj 1-containing neurites extending from the cell body.

To determine if the appearance of actin aggregations prior to neurite initiation was a general feature of multiple

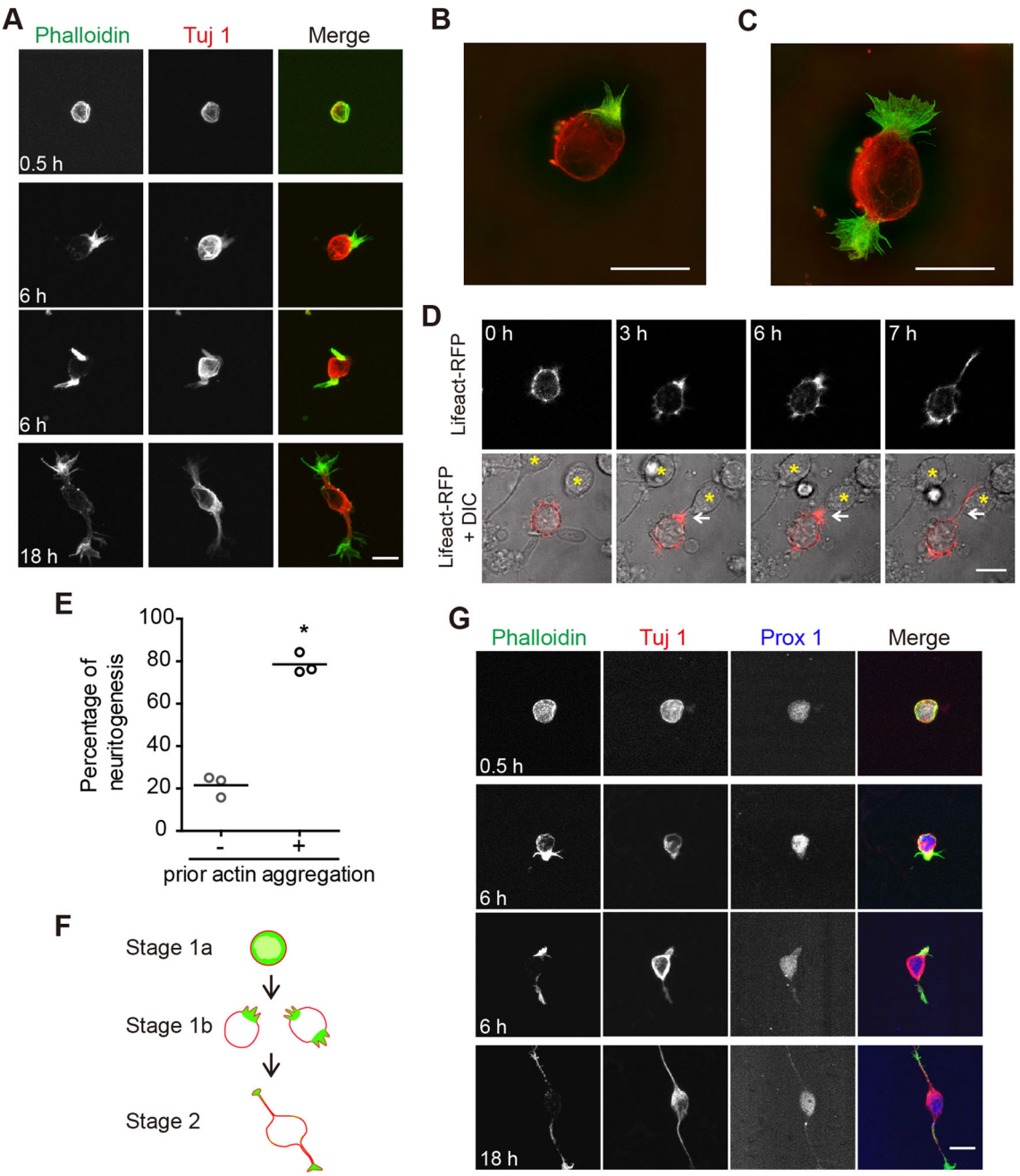

Fig. 1 Reorganization of evenly-distributed cortical actin into large aggregations precedes neurite initiation. **A** Representative images of cultured rat hippocampal neurons at different time points in culture. Fixed neurons were stained with Alexa-488 phalloidin (*green* in merge) and anti-Tuj 1 antibody (Alex-568, *red* in merge). **B, C** Large actin aggregations imaged using SIM; colors as in **A**. **D** Live-imaging time frames showing a neurite (arrow, 7 h) initiating from the site of a large actin aggregate, clearly present in previous frames (arrow, 3 and 6 h). F-actin labelled using Lifeact-RFP (*red*). *Yellow stars* indicate positions of neighboring, untransfected neurons. **E** Quantitation of live-imaging results in **D**. Three independent experiments, consisting of 75 neurites from 62 neurons, were quantified (paired two-tailed *t*-test $P < 0.05$). **F** Schematic of Stages 1a, 1b, and 2 of neuronal development. **G** Representative images of cultured rat dentate granule neurons at different developmental stages. Prox 1 is a granule neuron-specific marker (labelled with Alexa-633, *blue* in merge). Scale bars, 10 μm in all images.

cell types, we also immunostained hippocampal granule cells with phalloidin and Tuj 1, and found phenotypes and time courses of development very similar to hippocampal CA1 neurons. Specifically, we found that shortly after plating, neurons displayed a uniform actin cortex directly underneath the membrane (Fig. 1G, 0.5 h), while at 6 h after plating, neurons exhibited one or two actin aggregations and began to form short neurites (Fig. 1G, 6 h). By

18 h after plating, the first two neurites were typically formed, with actin growth cones at the tips of Tuj 1 immuno-positive neurites (Fig. 1G, 18 h).

Actin Stabilization Prevents Neurite Initiation

Our immunocytochemistry and live imaging results clearly demonstrated the presence of a thick actin cortex in newly-plated neurons prior to the formation of one or two large actin aggregations and neurite initiation from these sites. Is a breakage of symmetry in the initial actin cortex a pre-requisite for neurite initiation? To test this, we treated newly-plated neurons with different concentrations of jasplakinolide, a cell-permeable actin polymerizing and stabilizing drug. We found that 100 nmol/L or 1 μmol/L jasplakinolide significantly inhibited neuronal morphogenesis, while the lower concentration of 10 nmol/L did not have significant effects. At 6 h post-plating, all neurons in control cultures had entered either stage 1b or stage 2, while neurons treated with 100 nmol/L or 1 μmol/L jasplakinolide were mostly stuck in stage 1a, with only a small proportion of cells entering stage 1b (Fig. 2A, B). By 18 h after plating, all control neurons and those treated with 10 nmol/L jasplakinolide had reached stage 2, while those treated with higher concentrations of jasplakinolide had not significantly changed from their state at 6 h post-plating, still mostly stalled in stage 1a (Fig. 2A, B). The number of neurites (immuno-positive for Tuj 1) was also significantly reduced in neurons treated with 100 nmol/L or 1 μmol/L jasplakinolide, at both 6 and 18 h post-plating (Fig. 2C). In fact, while control neurons exhibited on average one neurite at 6 h post-plating and 3 neurites at 18 h post-plating, only 25% of neurons treated with 100 nmol/L or 1 μmol/L jasplakinolide had 1 neurite at 6 h post-plating and by 18 h post-plating, most jasplakinolide-treated neurons still did not extend neurites (26/40 cells for 100 nmol/L and 14/20 cells for 1 μmol/L; Fig 2A–C).

Actin Depolymerization Promotes Neurite Outgrowth

Having demonstrated an inhibitory role of actin stabilization in neurite initiation, we next tested the role of actin depolymerization, using latrunculin A, a pharmacological agent that disrupts F-actin formation by binding to globular actin (G-actin) at 1:1 stoichiometry. At 25 nmol/L, latrunculin A did not significantly affect the course of neuronal morphogenesis (Fig. 3A–C). Interestingly, treatment with higher concentrations, 250 nmol/L or 2.5 μmol/L, significantly accelerated neuronal morphogenesis, as almost all cells reached stage 2 by 6 h in culture, as compared with 75% in control cultures. The number of neurites was also significantly increased in neurons treated with latrunculin A (Fig. 3A–C).

To confirm these results, we treated neurons with cytochalasin D, an actin depolymerizing agent that binds to F-actin and prevents its further elongation. The results were very similar to those of latrunculin A treatment, in that a low concentration (100 nmol/L) of cytochalasin D had no significant effect, while higher concentrations significantly accelerated neuronal morphogenesis and increased neurite number at 6 h post-plating (Fig. 3D, E).

Thus, using two actin depolymerizing agents with different mechanisms of action, we demonstrated that the acceleration of actin depolymerization promoted neuronal morphogenesis and neurite formation. An intriguing question arising from the above results is that if actin depolymerization is sufficient for promoting neurite initiation, why did we observe actin aggregates prior to neurite initiation (Fig. 1)? To address this issue, we biochemically assayed the ratio of G-actin to F-actin in control neurons, as well as those treated with jasplakinolide or latrunculin A. In neurons treated with 100 nmol/L jasplakinolide, only F-actin was detectable (Fig. 4), suggesting that all actin molecules were effectively polymerized. In neurons treated with 2.5 μmol/L latrunculin A, on the other hand, although a significant increase in the G/F-actin ratio occurred following 6 h of treatment, high levels of F-actin were still present at both 6 and 18 h post-treatment (Fig. 4). Thus, even though latrunculin A promoted actin depolymerization, there was still sufficient F-actin left for marking the site of neurite initiation. These results are consistent with a critical role of actin dynamics, and specifically the formation of large actin aggregations, in neurite initiation.

Microtubule Dynamics Is Required for Neurite Extension

The extension of microtubules into actin-rich filopodia is a fundamental "next" step in neurite formation. Indeed, in our neuronal cultures, neurites emerging from large actin aggregations were Tuj 1 immuno-positive. To test the requirement for microtubule dynamics in neurite morphogenesis, we treated neurons with paclitaxel, a pharmacological agent that promotes the assembly of microtubules into stable, aggregated structures. In neurons treated with either 60 nmol/L or 6 μmol/L paclitaxel, neuritogenesis was decelerated to some degree, in that at 6 h, 27.5% of control neurons (11/40 cells) were at stage 1b, as compared with 62.5% or 66.7% of neurons (25/40 or 26/39 cells) treated with 60 nmol/L or 6 μmol/L paclitaxel, respectively (Fig. 5A, B). By 18 h post-plating, neurons under all treatment conditions reached stage 2 (Fig. 5A, B). This is in contrast to the effect of jasplakinolide treatment, where many neurons were still stalled in stage 1a by 18 h

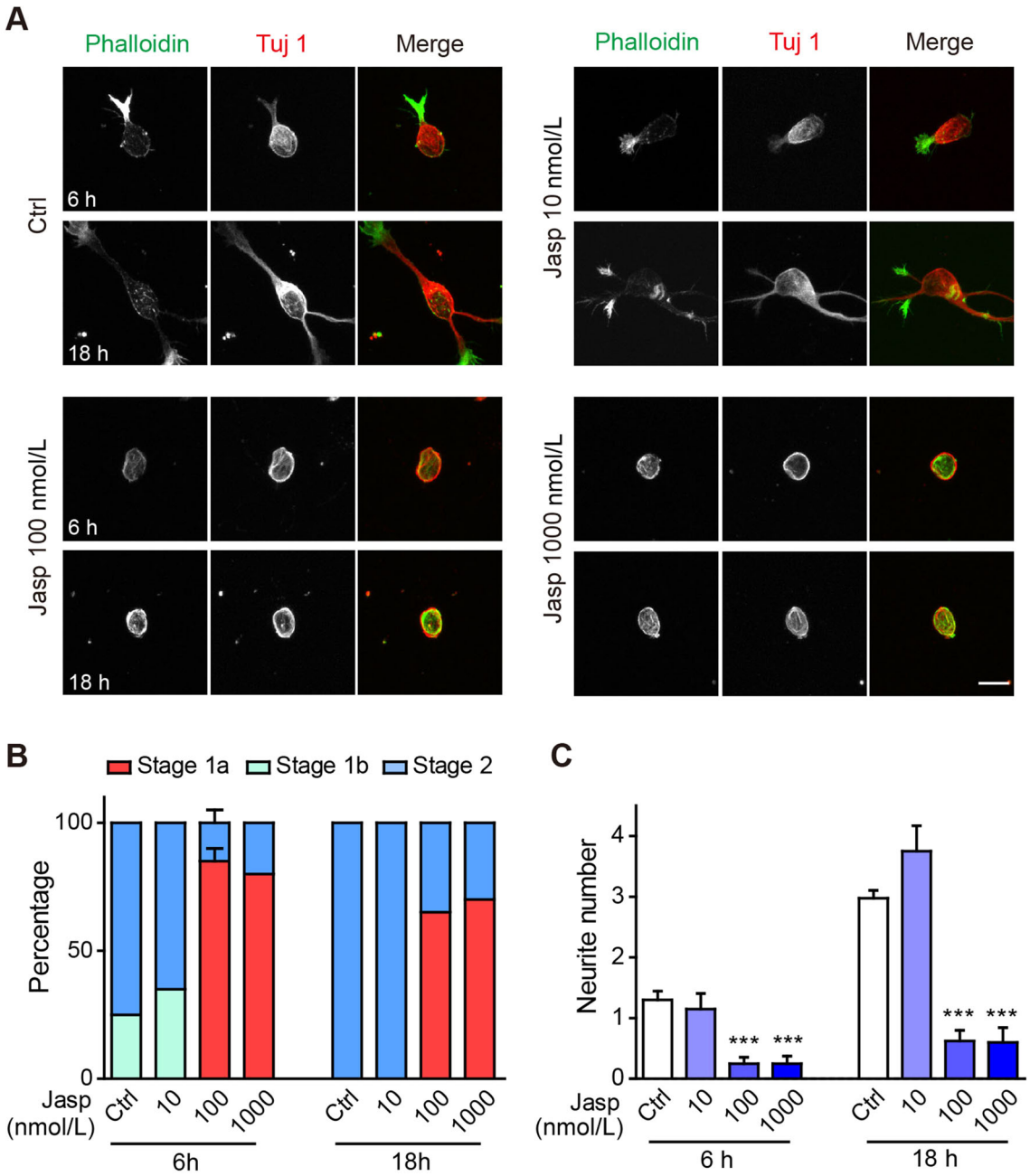

Fig. 2 Jasplakinolide treatment blocks actin reorganization and neurite initiation. **A** Representative images of neurons treated with vehicle (Ctrl), 10 nmol/L, 100 nmol/L, or 1000 nmol/L jasplakinolide (Jasp). Neurons were stained with Alexa-488 phalloidin (*green* in merge) and anti-Tuj 1 antibody (Alex-568, *red* in merge). Scale bar, 10 μm. **B**, **C** Quantification of neuronal developmental stages (**B**) and neurite number (**C**). $n = 40$ neurons for the Ctrl and 100 nmol/L jasplakinolide groups and 20 neurons for the other groups. In (**B**), the neuronal developmental stage distributions in Ctrl and 100 nmol/L jasplakinolide were significantly different both at 6 h (stage 1a ***, stage 1b **, stage 2 ***) and 18 h (stage 1a ***, stage 1b n.s., stage 2 ***) by two-way ANOVA, followed by Bonferroni post-tests (same statistical test used in all subsequent neuronal developmental stage quantification). In (**C**) , $***P < 0.001$ for the 100 and 1000 nmol/L jasplakinolide conditions, at both 6 and 18 h by one-way ANOVA, followed by Dunnett's multiple comparison test (same statistical test used in all subsequent neurite number or length quantification). In this and all subsequent images, error bars indicate s.e.m., $*P < 0.05$, $**P < 0.01$, $***P < 0.001$, n.s.: $P > 0.05$.

(Fig. 2B). Paclitaxel treatment also significantly reduced the number of neurites (Fig. 5C).

We next tested the effect of nocodazole, a microtubule destabilizing and depolymerizing agent. At 30 nmol/L, nocodazole did not significantly affect neuronal morphogenesis or neurite number (Fig. 5D, E). At the higher concentration of 3 μmol/L however, the proportion of neurons arrested at stage 1b increased at 6 h post-plating

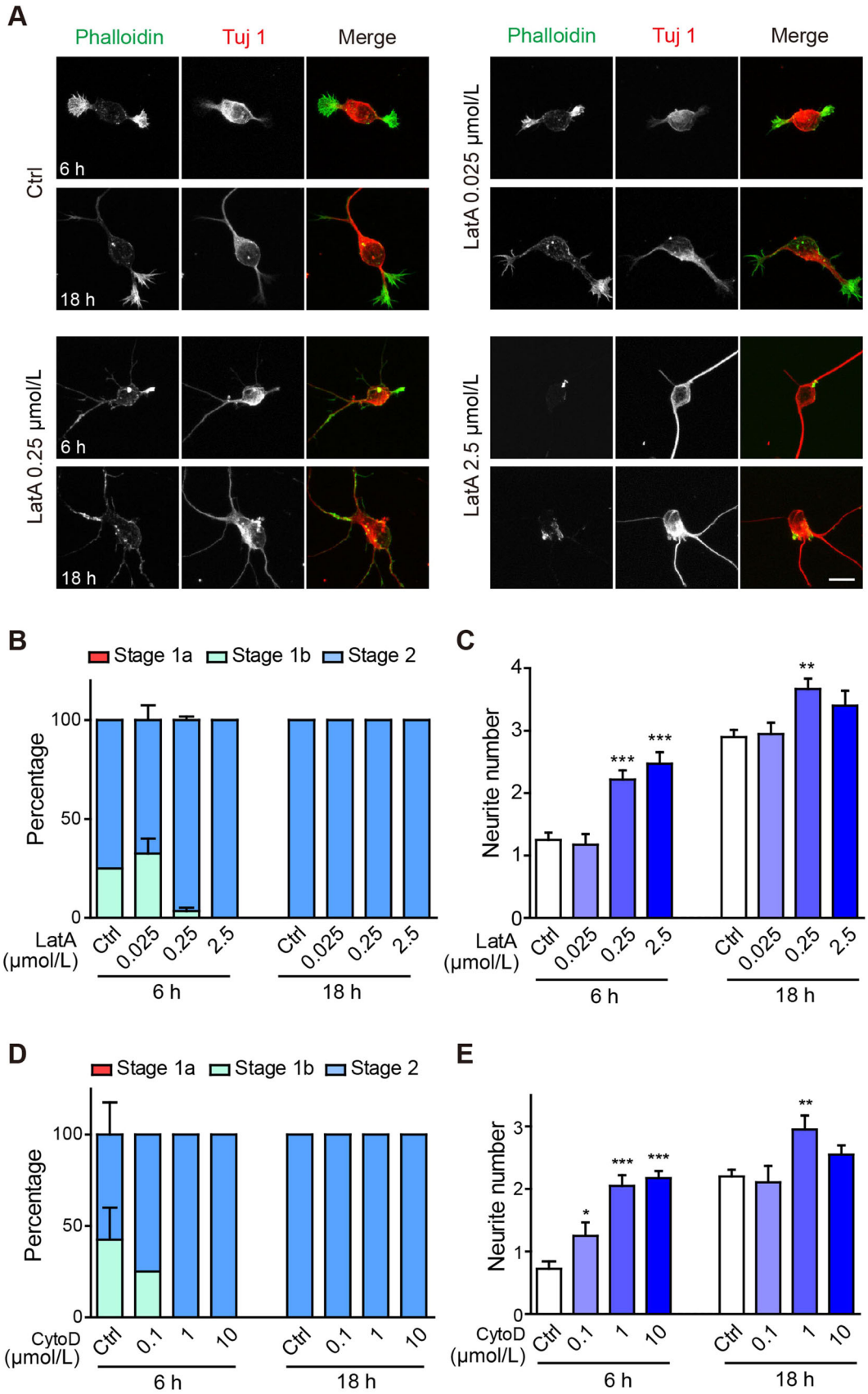
A
Phalloidin
Tuj 1
Merge
Ctrl
LatA 0.025 μmol/L
LatA 0.25 μmol/L
LatA 2.5 μmol/L
6 h
18 h
B
Stage 1a
Stage 1b
Stage 2
Percentage
LatA (μmol/L)
Ctrl
0.025
0.25
2.5
C
Neurite number
D
CytoD (μmol/L)
0.1
1
10
E

◀**Fig. 3** Latrunculin A or Cytochalasin D treatment accelerates neurite initiation. **A** Representative images of neurons treated with vehicle (Ctrl), 0.025 µmol/L, 0.25 µmol/L, or 2.5 µmol/L latrunculin A (LatA). Neurons were stained with Alexa-488 phalloidin (*green* in merge) and anti-Tuj 1 antibody (Alex-568, *red* in merge). Scale bar, 10 µm. **B**,**C** Quantification of neuronal developmental stages (**B**) and neurite number (**C**) of neurons shown in (**A**). $n = 60$ neurons for the Ctrl and 0.25 µmol/L latrunculin A groups and 40 neurons for the other groups. In (**B**), the 0.025 µmol/L LatA-treated neurons were n.s. relative to Ctrl, while both the 0.25 µmol/L and 2.5 µmol/L LatA groups showed accelerated growth to stage 2 at 6 h (both groups: stage 1a n.s., stage 1b ***, stage 2 *** by two-way ANOVA). All groups in the 18 h group were n.s. relative to Ctrl. **D**, **E** Quantification of neuronal developmental stages (**D**) and neurite number (**E**) of neurons treated with vehicle (Ctrl), 0.1 µmol/L, 1 µmol/L, or 10 µmol/L cytochalasin D (CytoD). $n = 40$ neurons for the Ctrl and 10 µmol/L cytochalasin D groups and 20 neurons for the other groups. **D** Neurons of the 10 µmol/L CytoD group showed accelerated growth to stage 2 at 6 h (stage 1a n.s., stage 1b **, stage 2 **) and were n.s. relative to Ctrl at 18 h by two-way ANOVA.

and was strikingly different at 18 h post-plating, where 50% of neurons (20/40 cells) had not yet reached stage 2, as compared to all cells completing this process in the control group (Fig. 5D). The number of neurites was also significantly reduced in neurons treated with 3 µmol/L nocodazole (Fig. 5E). We note that some nocodazole-treated neurons had multiple filopodial-like processes that were F-actin rich, but lacked Tuj 1 immunostaining, as if they had attempted to initiate multiple processes in the absence of microtubule invasion (Fig. 5A). These results, combined with those of paclitaxel treatment, demonstrate an important role of microtubule dynamics and/or function in regulating neurite morphogenesis, especially during the transition from stage 1b to stage 2, but not for that from stage 1a to 1b.

Protein Synthesis is Not Required for Neurite Initiation

In the above experiments, we showed that neurite morphogenesis initially required significant reorganization of the actin cytoskeleton, and at later stages, also changes in microtubules. Are these morphological changes mediated solely by rearrangements of existing proteins or do new proteins need to be synthesized? To test this, we treated neuronal cultures with the protein synthesis inhibitor cycloheximide (50 mg/mL). At 6 h and 18 h, neuronal development was not significantly affected (Fig. 6A-C), while at 18 h neurite number was significantly lower in cycloheximide-treated neurons (Fig. 6C). Thus, protein synthesis is specifically required for the later microtubule-dependent stages of neuritogenesis. Consistently, cycloheximide treatment did not significantly affect the G/F-actin ratio (Fig. 4).

Actin Dynamics during Cortical and Hippocampal Development *In Vivo*

Having demonstrated an early role of actin dynamics in early neuritogenesis during the transition from stage 1a to stage 1b, and a later effect of microtubules and protein synthesis in the transition from stage 1b to stage 2, we next asked if redistribution of the actin cytoskeleton also occurs *in vivo*. In both the cerebral cortex and hippocampus, neurons are born in the ventricular zone (VZ) and then migrate respectively to the cortical plate (CP) and stratum pyramidale (SP) [56, 57], with the net effect that neurons in the VZ/subventricular zone (SVZ) region are less mature than those in CP or SP. We thus *in utero* electroporated GFP-actinin, which binds to and crosslinks F-actin [52], together with cytoplasmic tdTomato, in E15.5 rat embryos and examined the F-actin distribution in neurons of the VZ/SVZ and CP/SP regions in E18.5 embryos. Consistent with our results in cultured neurons, we found that neurons in the VZ/SVZ regions of the cerebral cortex and CA1 hippocampus all had a thick layer of GFP-actinin surrounding the cell body, while those in the CP and SP had no detectable GFP-actinin fluorescence surrounding the cell body (Fig. 7A, B). In terms of both developmental stage and neurite number, neurons in the CP and SP regions were more mature than those in the VZ/SVZ (Fig. 7C, D).

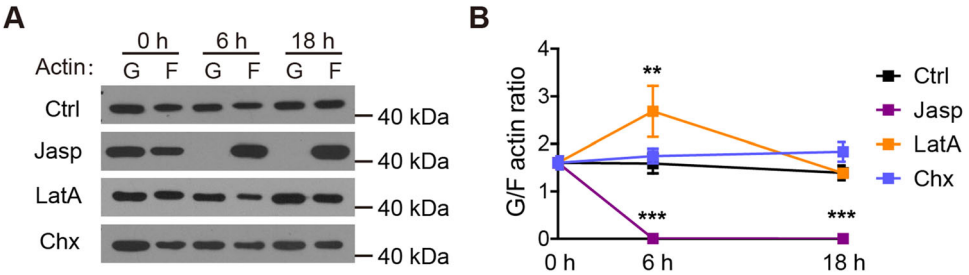

Fig. 4 Effect of inhibiting actin dynamics or protein synthesis on the G/F-actin ratio. **A** Western blots showing the G- and F-actin levels in neurons treated with vehicle (Ctrl), jasplakinolide (Jasp, 100 nmol/L), latrunculin A (LatA, 2.5 µmol/L), or cycloheximide (Chx, 50 mg/mL). **B** Quantitation of the data shown in (**A**). $n = 8$ for Ctrl, 2 for Jasp, 3 for LatA, and 5 for Chx, where n represents independent culture preparations. $^{**}P < 0.01$, $^{***}P < 0.001$, two-way ANOVA followed by Bonferroni post-tests.

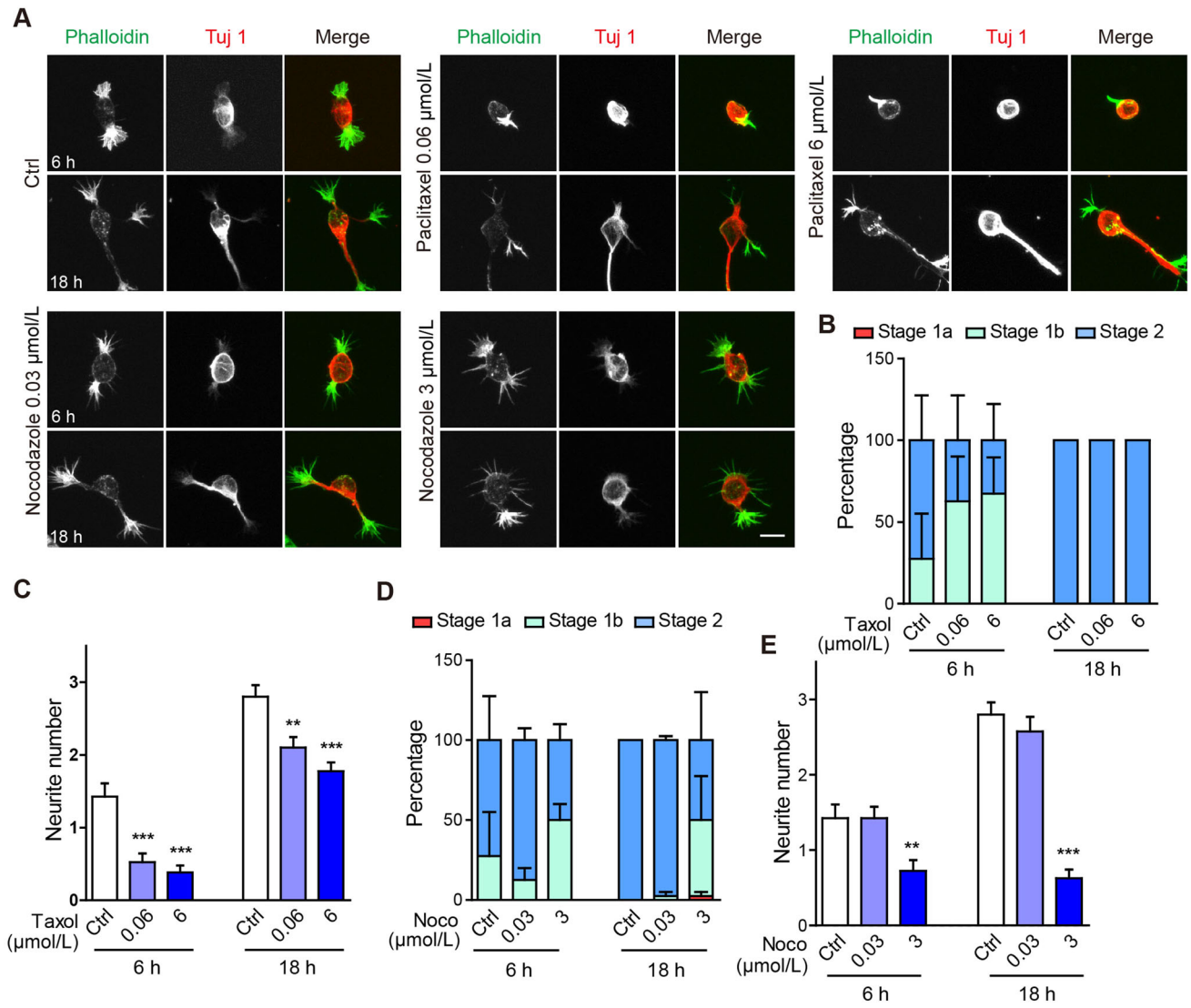

Fig. 5 Altering microtubule dynamics does not affect the transition from stage 1a to 1b, but significantly reduces neurite number. **A** Representative images of neurons treated with vehicle (Ctrl), 0.06 μmol/L paclitaxel (Taxol), 6 μmol/L paclitaxel, 0.03 μmol/L nocodazole (Noco), or 3 μmol/L nocodazole for 6 and 18 h. Neurons were stained with Alexa-488 phalloidin (*green* in merge) and anti-Tuj 1 antibody (Alex-568, *red* in merge). Scale bar, 10 μm. **B**, **C** Quantification of neuronal developmental stages (**B**) and neurite number (**C**) of neurons treated with paclitaxel for 6 h or 18 h. In (**B**), all conditions were n.s. compared with Ctrl. **D**, **E** Quantification of neuronal developmental stages (**D**) and primary neurite number (**E**) of neurons treated with nocodazole. In (**D**), all conditions were n.s. compared with Ctrl. $n = 40$ neurons for all groups.

Measuring GFP-actinin intensity along the circumference of each neuron's soma, normalized to that of tdTomato, we found significantly higher levels of GFP-actinin in immature neurons in the VZ/SVZ region, compared with more mature neurons in the CP and SP regions (Fig. 7E, F).

These findings were further confirmed by *in utero* electroporation of Lifeact-RFP, the high-affinity F-actin binding protein we used in the earlier live imaging experiments. Here, we also three-dimensionally reconstructed the neurons that we imaged to ensure that all processes extending from the cell body were visualized (Fig. 7G). Consistent with our GFP-actinin results, neurons in the CP region were more mature and had more neurites than those in the VZ (Fig. 7G–I).

Discussion

In the present study, through a combination of pharmacological and live-imaging approaches, we subdivided the process of neuritogenesis into two steps: (1) redistribution of cortical actin into one or two large actin aggregates (stage 1b); and (2) neurite extension from the sites of actin aggregation and growth of Tuj 1-filled neurites (stage 2).

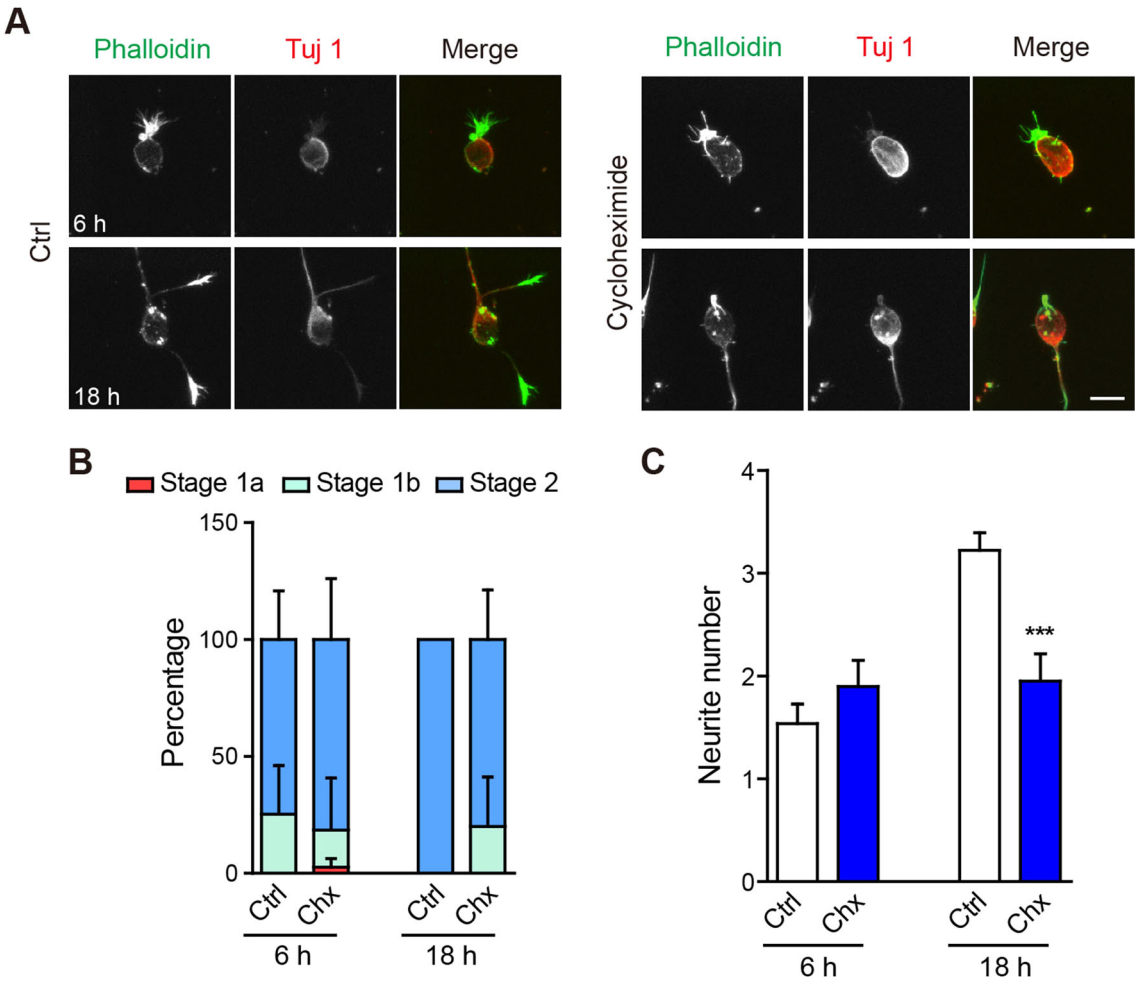

Fig. 6 Protein synthesis is not required for neurite initiation. **A** Representative images of neurons treated with vehicle (Ctrl) or 50 mg/mL cycloheximide (Chx) for 6 h or 18 h. Neurons were stained with Alexa-488 phalloidin (*green* in merge) and anti-Tuj1 antibody (Alex-568, *red* in merge). Scale bar, 10 μm. **B**, **C** Quantification of neuronal developmental stages (**B**) and neurite number (**C**) at 6 or 18 h. In (**B**), the Chx condition was n.s. relative to Ctrl at 6 or 18 h. $n = 40$ neurons in each group. $^{***}P < 0.001$, unpaired two-tailed t test.

We further demonstrated a critical role of actin depolymerization and redistribution in the transition from stage 1a to 1b, and a requirement for microtubule dynamics and protein synthesis in the transition from stage 1b to stage 2. Together, these results demonstrate an orderly sequence of events and requirement for different physiological factors during early neuritogenesis.

In the context of existing work investigating the role of the actin and microtubule cytoskeleton in neuritogenesis, we believe that our study makes the following contributions to the field. First, by examining the effects of actin and microtubule stabilizing and destabilizing agents on neuritogenesis, and using each agent over multiple concentrations to assess their dosage effect, we provide a systematic study of the relative contributions of actin and microtubules to neurite formation. These results complement those of previous studies using molecular tools to investigate the role of the actin cytoskeleton in neuritogenesis [41, 47, 48]. Our subdivision of stage 1 into stages 1a and 1b helps to clarify the need for both actin depolymerization and actin polymerization in neurite initiation (Figs. 1, 2, 3 and 4). These results were further confirmed *in vivo* using two F-actin binding probes, Actinin-GFP and Lifeact-RFP (Fig. 7).

Second, in terms of microtubule dynamics, we showed that this was specifically required for the formation of stable neurites during the transition from stage 1b to 2. Here, dynamics is the key, as microtubule stabilization with paclitaxel or depolymerization with nocodazole both resulted in reduced neurite numbers (Fig. 5). The difference between the two drug treatments is that neurons treated with paclitaxel (6 μmol/L, Fig. 5A) had large-diameter neurites, while those treated with nocodazole (3 μmol/L, Fig. 5A) extended many thin filopodia lacking

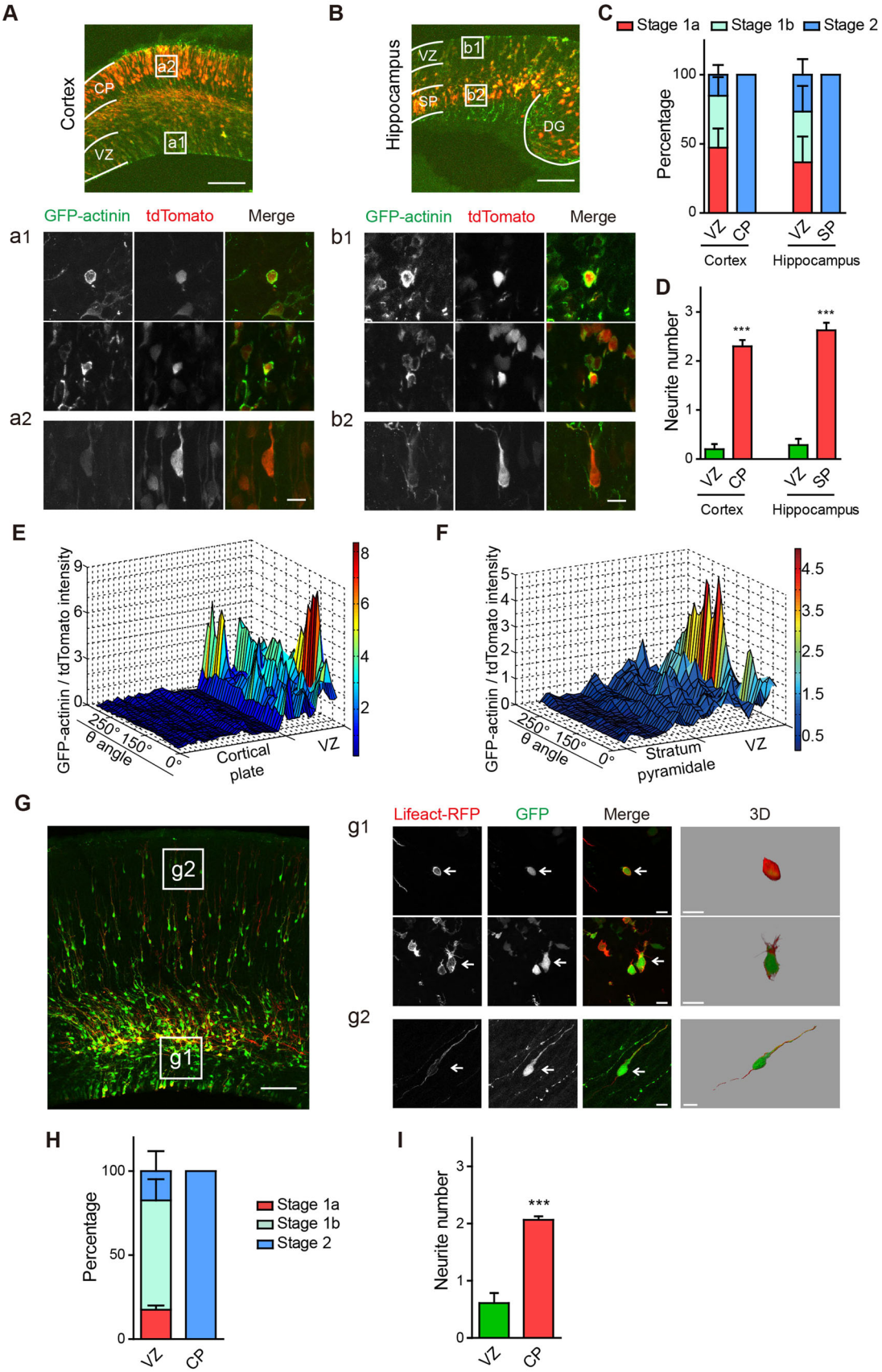
A
Cortex
CP
VZ
a2
a1
B
Hippocampus
VZ
SP
DG
b1
b2
C
Stage 1a
Stage 1b
Stage 2
Percentage
100
50
0
VZ
CP
SP
Cortex
Hippocampus
GFP-actinin
tdTomato
Merge
a1
a2
b1
b2
D
Neurite number
***
E
GFP-actinin / tdTomato intensity
θ angle
250°
150°
0°
Cortical plate
VZ
F
Stratum pyramidale
G
g1
g2
Lifeact-RFP
GFP
3D
H
I

◀**Fig. 7** Cortical actin reorganization also occurs before neurite initiation *in vivo*. **A**, **B** Representative images of rat cerebral cortex (**A**) and hippocampus (**B**) at E18.5. Neurons were electroporated *in utero* with tdTomato (*red*) and GFP-actinin (*green*). DG, dentate gyrus; scale bar, 100 μm. (*a1*, *b1*, *a2*, *b2*) Representative images of neurons in the VZ (*a1*, *b1*), CP (*a2*), and SP (*b2*). Scale bar, 10 μm. **C**, **D** Quantification of developmental stages (**C**) and neurite number (**D**) of neurons in (**A**, **B**). In (**C**), VZ neurons were at earlier stages than in the CP and SP (VZ *vs* CP: stage 1a **, stage 1b *, stage 2 ***; VZ *vs* SP: stage 1a n.s., stage 1b n.s., stage 2 ***; $n = 14$-20 neurons per condition; ***$P < 0.001$, unpaired two-tailed *t* test). **E**, **F** Quantification of GFP-actinin intensity in neurons, normalized to that of tdTomato, in the cerebral cortex (**E**) and hippocampus (**F**). $n = 10$–20 neurons per condition. **G** Representative image of the rat cerebral cortex at E18.5, electroporated with Lifeact-RFP (*red*) and GFP (*green*). Scale bar, 100 μm. (*g1*, *g2*) Representative images of neurons in the VZ (*g1*) and CP (*g2*). Scale bar, 10 μm. The rightmost panels in (*g1*) and (*g2*) are magnified and 3D-rendered views of the example neurons marked by arrows. **H**, **I** Quantification of developmental stages (**H**) and neurite number (**I**) of neurons in (**G**). **H** VZ neurons were at earlier stages than in the CP (stage 1a n.s., stage 1b ***, stage 2 ***). $n = 16$ neurons for VZ and 23 for CP. **D**, **I** ***$P < 0.001$, unpaired two-tailed *t* test.

Tuj 1 immunostaining, as if they keep attempting to extend more processes in the absence of stabilized ones. Since microtubules, in addition to their cytoskeletal functions, are also critical for polarized cargo transport along neurites, some of the effects observed may also be attributed to the cargos carried along microtubules by associated motor proteins [58–60].

Finally, by examining the role of protein synthesis in neuritogenesis in the same culture system as actin and microtubule dynamics, we demonstrated that protein synthesis was strictly required for microtubule-dependent neurite extension during the transition from stage 1b to stage 2, but not during actin-dependent neurite initiation during the transition from stage 1a to 1b.

Our results, together with those of previous studies [41, 47, 48], pose the next interesting question, namely, what signal initiates the formation of actin aggregations? Since actin aggregations form within the cell and at physical locations close to the cell membrane, they could either be initiated by intrinsic, membrane-associated cues, or extracellular cues that signal *via* transmembrane receptors. Based on previous studies on related physiological processes, several classes of candidate molecules come into view. (1) Extracellular cues or neurotrophic factors: the guidance molecule semaphorin 3A has been shown to promote the formation of the apical dendrite in pyramidal neurons [69], while brain-derived neurotrophic factor has been shown to promote axon differentiation and dendrite growth [70, 71]. (2) Cell adhesion molecules: N-cadherin has been reported to be asymmetrically distributed during early neuronal development, in one of the earliest events during the establishment of asymmetry [48, 72]. (3) Phosphorylated derivatives of the phospholipid phosphatidylinositol or phosphoinositides: as membrane-localized signaling molecules which interact with the actin cytoskeleton [73, 74], PIP3, a member of this family, has been shown to promote neuronal polarization [75, 76] and the formation of axonal filopodia [77].

We propose that one of the above-mentioned cues, or at least one with such a function, signals the change of state from a thick and evenly-distributed actin cortex in stage 1a to one or two large aggregations in stage 1b. Although both stages 1a and 1b are rich in F-actin, actin dynamics is required for the transition, a process completely blocked by jasplakinolide. Actin dynamics is further required for neurite outgrowth and the transition from stage 1b to 2.

How does the accumulation of F-actin lead to neurite initiation? It has been proposed that microtubule-associated proteins that can also interact with actin, such as MAP2c, promote neurite extension by facilitating microtubule assembly and extension at the sites of actin aggregates [34, 38, 39, 41, 47, 78, 79]. Similar effects have also been reported for the F-actin-associated protein drebrin, which has recently been shown to bind to the microtubule plus-end protein EB3 and also promote neuritogenesis [80]. Related to the above molecular mechanisms, the radial actin bundles assembled at the sites of actin aggregates in stage 1b are also likely to be structurally permissive for microtubule assembly and extension [41, 47].

The process underlying the formation of actin aggregates and subsequent filopodial extension is also shared with non-neuronal cells, which can extend actin-rich filopodia and short protrusions as sensors and leading processes during motility and chemotaxis [31, 33, 64]. In terms of molecular mechanisms, eukaryotic chemotaxis requires actin remodeling *via* actin-associated proteins to form actin aggregates or clusters, followed by short protrusions, in a process very similar to neuritogenesis [66–68]. Why then do non-neuronal cells not extend neurites? We speculate that this is likely due to the lack of high levels of microtubule-associated proteins, such as MAP2c. Previous work has shown that over-expression of MAP2c in neuroblastoma cell lines induce neurite formation [34, 38], demonstrating that MAP2c, or proteins with similar functions, are capable of converting filopodia in non-neuronal cells into neurite-like processes. Thus, although neurons are highly specialized cell types with distinct morphologies and functions, they share many of their basic cell biological mechanisms, including the formation of actin aggregates and the extension of cellular processes, with other cell types.

Acknowledgments We thank Yuan Lu, Zong-Fang Wan, and Shun-Ji He for excellent technical assistance. We thank the ION Optical Imaging Core Facility for technical support, and the IOBS-Nikon

Biological Imaging Center for use of the N-SIM microscope. We are grateful to colleagues at ION and members of the Yu laboratory for suggestions and comments. This work was supported by grants from the National Natural Science Foundation of China (31125015 and 31321091).

References

1. Dotti CG, Sullivan CA, Banker GA. The establishment of polarity by hippocampal neurons in culture. J Neurosci 1988, 8: 1454–1468.
2. Craig AM, Banker G. Neuronal polarity. Annu Rev Neurosci 1994, 17: 267–310.
3. Barnes AP, Solecki D, Polleux F. New insights into the molecular mechanisms specifying neuronal polarity *in vivo*. Curr Opin Neurobiol 2008, 18: 44–52.
4. Funahashi Y, Namba T, Nakamuta S, Kaibuchi K. Neuronal polarization *in vivo*: Growing in a complex environment. Curr Opin Neurobiol 2014, 27: 215–223.
5. Randlett O, Norden C, Harris WA. The vertebrate retina: a model for neuronal polarization *in vivo*. Dev Neurobiol 2011, 71: 567–583.
6. Arimura N, Kaibuchi K. Neuronal polarity: from extracellular signals to intracellular mechanisms. Nat Rev Neurosci 2007, 8: 194–205.
7. Barnes AP, Polleux F. Establishment of axon-dendrite polarity in developing neurons. Annu Rev Neurosci 2009, 32: 347–381.
8. Cheng PL, Poo MM. Early events in axon/dendrite polarization. Annu Rev Neurosci 2012, 35: 181–201.
9. Stiess M, Bradke F. Neuronal polarization: the cytoskeleton leads the way. Dev Neurobiol 2011, 71: 430–444.
10. Arikkath J. Molecular mechanisms of dendrite morphogenesis. Front Cell Neurosci 2012, 6: 61.
11. Cline H, Haas K. The regulation of dendritic arbor development and plasticity by glutamatergic synaptic input: a review of the synaptotrophic hypothesis. J Physiol 2008, 586: 1509–1517.
12. Koleske AJ. Molecular mechanisms of dendrite stability. Nat Rev Neurosci 2013, 14: 536–550.
13. Puram SV, Bonni A. Cell-intrinsic drivers of dendrite morphogenesis. Development 2013, 140: 4657–4671.
14. Urbanska M, Blazejczyk M, Jaworski J. Molecular basis of dendritic arborization. Acta Neurobiol Exp (Wars) 2008, 68: 264–288.
15. Jan YN, Jan LY. Branching out: mechanisms of dendritic arborization. Nat Rev Neurosci 2010, 11: 316–328.
16. Wong RO, Ghosh A. Activity-dependent regulation of dendritic growth and patterning. Nat Rev Neurosci 2002, 3: 803–812.
17. Dalva MB, McClelland AC, Kayser MS. Cell adhesion molecules: signalling functions at the synapse. Nat Rev Neurosci 2007, 8: 206–220.
18. McAllister AK. Dynamic aspects of CNS synapse formation. Annu Rev Neurosci 2007, 30: 425–450.
19. Shen K, Scheiffele P. Genetics and cell biology of building specific synaptic connectivity. Annu Rev Neurosci 2010, 33: 473–507.
20. Waites CL, Craig AM, Garner CC. Mechanisms of vertebrate synaptogenesis. Annu Rev Neurosci 2005, 28: 251–274.
21. Yuste R, Bonhoeffer T. Genesis of dendritic spines: insights from ultrastructural and imaging studies. Nat Rev Neurosci 2004, 5: 24–34.
22. Bhatt DH, Zhang S, Gan WB. Dendritic spine dynamics. Annu Rev Physiol 2009, 71: 261–282.
23. Holtmaat A, Svoboda K. Experience-dependent structural synaptic plasticity in the mammalian brain. Nat Rev Neurosci 2009, 10: 647–658.
24. Tada T, Sheng M. Molecular mechanisms of dendritic spine morphogenesis. Curr Opin Neurobiol 2006, 16: 95–101.
25. da Silva JS, Dotti CG. Breaking the neuronal sphere: regulation of the actin cytoskeleton in neuritogenesis. Nat Rev Neurosci 2002, 3: 694–704.
26. Flynn KC. The cytoskeleton and neurite initiation. Bioarchitecture 2013, 3: 86–109.
27. Sainath R, Gallo G. Cytoskeletal and signaling mechanisms of neurite formation. Cell Tissue Res 2014.
28. Zolessi FR, Poggi L, Wilkinson CJ, Chien CB, Harris WA. Polarization and orientation of retinal ganglion cells *in vivo*. Neural Dev 2006, 1: 2.
29. Namba T, Kibe Y, Funahashi Y, Nakamuta S, Takano T, Ueno T, *et al*. Pioneering axons regulate neuronal polarization in the developing cerebral cortex. Neuron 2014, 81: 814–829.
30. Hatanaka Y, Yamauchi K. Excitatory cortical neurons with multipolar shape establish neuronal polarity by forming a tangentially oriented axon in the intermediate zone. Cereb Cortex 2013, 23: 105–113.
31. Gupton SL, Gertler FB. Filopodia: the fingers that do the walking. Sci STKE 2007, 2007: re5.
32. Gallo G. Mechanisms underlying the initiation and dynamics of neuronal filopodia: from neurite formation to synaptogenesis. Int Rev Cell Mol Biol 2013, 301: 95–156.
33. Mattila PK, Lappalainen P. Filopodia: molecular architecture and cellular functions. Nat Rev Mol Cell Biol 2008, 9: 446–454.
34. Edson K, Weisshaar B, Matus A. Actin depolymerisation induces process formation on MAP2-transfected non-neuronal cells. Development 1993, 117: 689–700.
35. Caceres A, Mautino J, Kosik KS. Suppression of MAP2 in cultured cerebellar macroneurons inhibits minor neurite formation. Neuron 1992, 9: 607–618.
36. Smith CL. The initiation of neurite outgrowth by sympathetic neurons grown in vitro does not depend on assembly of microtubules. J Cell Biol 1994, 127: 1407–1418.
37. Teng J, Takei Y, Harada A, Nakata T, Chen J, Hirokawa N. Synergistic effects of MAP2 and MAP1B knockout in neuronal migration, dendritic outgrowth, and microtubule organization. J Cell Biol 2001, 155: 65–76.
38. Dehmelt L, Smart FM, Ozer RS, Halpain S. The role of microtubule-associated protein 2c in the reorganization of microtubules and lamellipodia during neurite initiation. J Neurosci 2003, 23: 9479–9490.
39. Dehmelt L, Halpain S. Actin and microtubules in neurite initiation: are MAPs the missing link? J Neurobiol 2004, 58: 18–33.
40. Marsh L, Letourneau PC. Growth of neurites without filopodial or lamellipodial activity in the presence of cytochalasin B. J Cell Biol 1984, 99: 2041–2047.
41. Dent EW, Kwiatkowski AV, Mebane LM, Philippar U, Barzik M, Rubinson DA, *et al*. Filopodia are required for cortical neurite initiation. Nat Cell Biol 2007, 9: 1347–1359.
42. Kwiatkowski AV, Rubinson DA, Dent EW, Edward van Veen J, Leslie JD, Zhang J, *et al*. Ena/VASP Is Required for neuritogenesis in the developing cortex. Neuron 2007, 56: 441–455.
43. Barzik M, Kotova TI, Higgs HN, Hazelwood L, Hanein D, Gertler FB, *et al*. Ena/VASP proteins enhance actin polymerization in the presence of barbed end capping proteins. J Biol Chem 2005, 280: 28653–28662.
44. Bear JE, Svitkina TM, Krause M, Schafer DA, Loureiro JJ, Strasser GA, *et al*. Antagonism between Ena/VASP proteins and actin filament capping regulates fibroblast motility. Cell 2002, 109: 509–521.

45. Andrianantoandro E, Pollard TD. Mechanism of actin filament turnover by severing and nucleation at different concentrations of ADF/cofilin. Mol Cell 2006, 24: 13–23.
46. Bernstein BW, Bamburg JR. ADF/cofilin: a functional node in cell biology. Trends Cell Biol 2010, 20: 187–195.
47. Flynn KC, Hellal F, Neukirchen D, Jacob S, Tahirovic S, Dupraz S, *et al*. ADF/cofilin-mediated actin retrograde flow directs neurite formation in the developing brain. Neuron 2012, 76: 1091–1107.
48. Gartner A, Fornasiero EF, Valtorta F, Dotti CG. Distinct temporal hierarchies in membrane and cytoskeleton dynamics precede the morphological polarization of developing neurons. J Cell Sci 2014, 127: 4409–4419.
49. Tan ZJ, Peng Y, Song HL, Zheng JJ, Yu X. N-cadherin-dependent neuron-neuron interaction is required for the maintenance of activity-induced dendrite growth. Proc Natl Acad Sci U S A 2010, 107: 9873–9878.
50. Yu X, Malenka RC. Beta-catenin is critical for dendritic morphogenesis. Nat Neurosci 2003, 6: 1169–1177.
51. Gallardo G, Schluter OM, Sudhof TC. A molecular pathway of neurodegeneration linking alpha-synuclein to ApoE and Abeta peptides. Nat Neurosci 2008, 11: 301–308.
52. Edlund M, Lotano MA, Otey CA. Dynamics of alpha-actinin in focal adhesions and stress fibers visualized with alpha-actinin-green fluorescent protein. Cell Motil Cytoskeleton 2001, 48: 190–200.
53. Rompani SB, Cepko CL. Retinal progenitor cells can produce restricted subsets of horizontal cells. Proc Natl Acad Sci U S A 2008, 105: 192–197.
54. Zheng JJ, Li SJ, Zhang XD, Miao WY, Zhang D, Yao H, *et al*. Oxytocin mediates early experience-dependent cross-modal plasticity in the sensory cortices. Nat Neurosci 2014, 17: 391–399.
55. He S, Ma J, Liu N, Yu X. Early enriched environment promotes neonatal GABAergic neurotransmission and accelerates synapse maturation. J Neurosci 2010, 30: 7910–7916.
56. Kriegstein AR, Noctor SC. Patterns of neuronal migration in the embryonic cortex. Trends Neurosci 2004, 27: 392–399.
57. Hayashi K, Kubo K, Kitazawa A, Nakajima K. Cellular dynamics of neuronal migration in the hippocampus. Front Neurosci 2015, 9: 135.
58. Hirokawa N, Niwa S, Tanaka Y. Molecular motors in neurons: transport mechanisms and roles in brain function, development, and disease. Neuron 2010, 68: 610–638.
59. Kapitein LC, Hoogenraad CC. Which way to go? Cytoskeletal organization and polarized transport in neurons. Mol Cell Neurosci 2011, 46: 9–20.
60. Namba T, Nakamuta S, Funahashi Y, Kaibuchi K. The role of selective transport in neuronal polarization. Dev Neurobiol 2011, 71: 445–457.
61. Kuijpers M, Hoogenraad CC. Centrosomes, microtubules and neuronal development. Mol Cell Neurosci 2011, 48: 349–358.
62. Xiao S, Jan LY. A gate keeper for axonal transport. Cell 2009, 136: 996–998.
63. Hirokawa N, Takemura R. Molecular motors in neuronal development, intracellular transport and diseases. Curr Opin Neurobiol 2004, 14: 564–573.
64. Heckman CA, Plummer HK, 3rd. Filopodia as sensors. Cell Signal 2013, 25: 2298–2311.
65. Edson K, Weisshaar B, Matus A. Actin Depolymerization Induces Process Formation on Map2-Transfected Nonneuronal Cells. Development 1993, 117: 689–700.
66. Graziano BR, Weiner OD. Self-organization of protrusions and polarity during eukaryotic chemotaxis. Curr Opin Cell Biol 2014, 30: 60–67.
67. Rougerie P, Miskolci V, Cox D. Generation of membrane structures during phagocytosis and chemotaxis of macrophages: role and regulation of the actin cytoskeleton. Immunol Rev 2013, 256: 222–239.
68. Wu D. Signaling mechanisms for regulation of chemotaxis. Cell Res 2005, 15: 52–56.
69. Polleux F, Morrow T, Ghosh A. Semaphorin 3A is a chemoattractant for cortical apical dendrites. Nature 2000, 404: 567–573.
70. Shelly M, Cancedda L, Heilshorn S, Sumbre G, Poo MM. LKB1/STRAD promotes axon initiation during neuronal polarization. Cell 2007, 129: 565–577.
71. McAllister AK, Katz LC, Lo DC. Opposing roles for endogenous BDNF and NT-3 in regulating cortical dendritic growth. Neuron 1997, 18: 767–778.
72. Gartner A, Fornasiero EF, Munck S, Vennekens K, Seuntjens E, Huttner WB, *et al*. N-cadherin specifies first asymmetry in developing neurons. EMBO J 2012, 31: 1893–1903.
73. Janmey PA, Lindberg U. Cytoskeletal regulation: rich in lipids. Nat Rev Mol Cell Biol 2004, 5: 658–666.
74. Saarikangas J, Zhao H, Lappalainen P. Regulation of the actin cytoskeleton-plasma membrane interplay by phosphoinositides. Physiol Rev 2010, 90: 259–289.
75. Shi SH, Jan LY, Jan YN. Hippocampal neuronal polarity specified by spatially localized mPar3/mPar6 and PI 3-kinase activity. Cell 2003, 112: 63–75.
76. Jiang H, Guo W, Liang X, Rao Y. Both the establishment and the maintenance of neuronal polarity require active mechanisms: critical roles of GSK-3beta and its upstream regulators. Cell 2005, 120: 123–135.
77. Ketschek A, Gallo G. Nerve growth factor induces axonal filopodia through localized microdomains of phosphoinositide 3-kinase activity that drive the formation of cytoskeletal precursors to filopodia. J Neurosci 2010, 30: 12185–12197.
78. Kim H, Binder LI, Rosenbaum JL. The periodic association of MAP2 with brain microtubules in vitro. J Cell Biol 1979, 80: 266–276.
79. Schaefer AW, Kabir N, Forscher P. Filopodia and actin arcs guide the assembly and transport of two populations of microtubules with unique dynamic parameters in neuronal growth cones. J Cell Biol 2002, 158: 139–152.
80. Geraldo S, Khanzada UK, Parsons M, Chilton JK, Gordon-Weeks PR. Targeting of the F-actin-binding protein drebrin by the microtubule plus-tip protein EB3 is required for neuritogenesis. Nat Cell Biol 2008, 10: 1181–1189.